# Prediction of Wave Loads with Measured Unsteady Pressure Distribution on Ship-Hull Surface

**Masashi Kashiwagi**[*], **Hidetsugu Iwashita**[**],
**Kurniawan T. Waskito**[*] **and Munehiko Hinatsu**[*]

[*] Dept of Naval Architecture & Ocean Engineering, Osaka University, Japan
[**] Dept of Transportation & Environmental Systems, Hiroshima University, Japan
*E-mail: kashi@naoe.eng.osaka-u.ac.jp*

## 1 INTRODUCTION

Prediction of wave loads on a ship is of vital importance for evaluating the ship's structural strength in waves. In the measurement of wave loads so far in a towing tank, segmented ship models have been used, with which the wave loads only at segmented sections could be measured with load cell installed. However, we need to obtain the longitudinal distribution of wave loads on a ship with higher accuracy; which could be realized by measuring the spatial distribution of unsteady pressure on the whole ship-hull surface and by properly integrating it in conjunction with measurement of ship motions in waves.

For that purpose, we use the data of unsteady pressure distribution measured in 2018 by means of a large number of FBG (Fiber Bragg Gratings) pressure sensors[1)] and at the same time the data of wave-induced ship motions and ship-side wave profile. In the experiment in 2018, we used 333 FBG pressure sensors affixed only on the port side of a ship, among which 70 sensors were placed above the still waterline. Using these measured data, a study is made in this paper on the wave-load distribution, and a comparison is also made with computed values using RPM (Rankine Panel Method) developed by Iwashita *et al.*[2)] and a CFD commercial software FINE/Marine to see nonlinear effects and features in the vertical bending moment.

## 2 OVERVIEW OF EXPERIMENT IN 2018

In the experiment in 2018, we used the RIOS (Research Initiative on Oceangoing Ships) bulk carrier[1)2)] whose principal particulars are shown in Table 1. Fig. 1 shows the body plan and also the position of pressure sensors, in which totally 333 FBG pressure sensors (including 70 sensors above the still waterline) were affixed on the port side and 19 strain-type pressure sensors were embedded in the starboard side (at ordinate numbers 5.0, 9.0 and 9.5, indicated by green-color square symbol in Fig. 1) to check the measurement accuracy of the FBG pressure sensors.

Table 1 Principal particulars of RIOS bulk carrier

| | |
|---|---|
| $L_{pp}$ (m) | 2.400 |
| $B$ (m) | 0.400 |
| $d$ (m) | 0.128 |
| $C_b$ | 0.800 |
| $C_w$ | 0.870 |
| $x_G$ (m) | 0.051 |
| $z_G$ (m) | −0.020 |
| $z_B$ (m) | −0.0618 |
| $\kappa_{yy}/L$ | 0.250 |

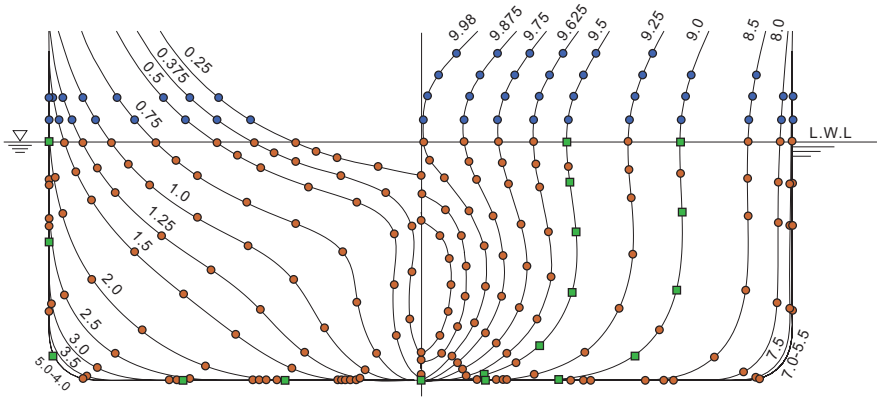


Fig. 1 Position of pressure sensors attached on RIOS bulk carrier.

The experiment was conducted at $Fn = 0.0$ and 0.18 in head waves with motion-free condition, measuring not only the pressure but also wave-induced ship motions (surge, heave and pitch). In addition, the ship-side wave, i.e. the wave profile on the ship-hull surface, was measured using capacitance-type wave gauges which were installed on another ship model made of urethane with the same geometry and dimensions. Since these

wave gauges were set along the girth with small separation gap from the hull surface and at the same transverse sections as those for measuring the pressure, we can detect the correct wetted surface of ship hull at each time instant, which is important for the pressure integration over the ship-hull surface and for computing resultant hydrodynamic forces. Furthermore, for a fundamental check, the measurement of pressure distribution has been performed for the diffraction (with motion fixed in wave) and radiation (with prescribed motions in calm water) problems, together with direct measurement of the total force by a dynamometer.

## 3 THEORETICAL BACKGROUNDS

The wave loads normally refer to the shear force and bending moment, but in this paper attention is focused on the vertical bending moment (VBM hereafter). There are two components in VBM owing to the integration of unsteady pressure and the inertia force. Thus the time-variant VBM acting on the transverse section at $x = x_0$ in the ship's longitudinal direction may be computed from

$$M_v(x_0) = \int_{x_A}^{x_0} dx \int_{C_H(x)} (P_D + P_R + P_S)\, n_5\, d\ell - \int_{x_A}^{x_0} \frac{w(x)}{g}(x - \ell_x - x_0)\{\ddot{\xi}_3 - (x - \ell_x)\ddot{\xi}_5\}\, dx, \tag{1}$$

where

$$n_5 = (z - \ell_z)n_1 - (x - \ell_x - x_0)n_3 = n_5^G + x_0 n_3, \tag{2}$$

with the origin of the coordinates taken at the center of gravity, denoted as $(\ell_x, 0, \ell_z)$ and the positive $z$-axis taken vertically upward. The hogging moment is defined to be positive in the VBM. $P_D$ and $P_R$ in Eq. (1) represent the diffraction and radiation pressures, respectively, and $P_S$ denotes the variation of hydrostatic pressure due to heave and pitch motions. In reality, the sum of these pressures is measured directly in the case of motion free in waves as a function of time and coordinates on the ship hull. $x_0$ denotes an arbitrary cross section where the VBM is to be computed, $x_A$ the longitudinal position of aft end of a ship, and $C_H(x)$ the contour of transverse section at station $x$.

The second line in Eq. (1) indicates the inertia-force term, where $\ddot{\xi}_3$ and $\ddot{\xi}_5$ are the acceleration in heave and pitch, respectively, and $w(x)$ is the weight-distribution function related to the ship's mass $m$ and the gyrational radius in pitch $\kappa_{yy}$ as follows:

$$\int_{x_A}^{x_F} \frac{w(x)}{g}\, dx = m, \quad \int_{x_A}^{x_F} \frac{w(x)}{g} x\, dx = m\ell_x, \quad \int_{x_A}^{x_F} \frac{w(x)}{g}(x - \ell_x)^2 dx = m\kappa_{yy}^2, \tag{3}$$

where $x_F$ in the upper limit of integration range denotes the fore end of a ship.

In calculating the VBM according to Eq. (1), the integrated result up to $x_0 = x_F$ must be consistent to the equations of coupled motion equations in surge, heave, and pitch. Namely the integrated value of Eq. (1) up to $x_0 = x_F$ must be equal to zero. In order to ensure this condition of zero VBM at the fore end of a ship and the correct computation of VBM in the time domain, the origin in time histories (i.e. the phase with respect to an incident wave) of both unsteady pressure and ship motions in Eq. (1) must be synchronized. In the present study, the VBM due to inertia force is computed under the assumption of uniform structural density; that is, the weight distribution is assumed equal to the distribution of volume displacement.

## 4 RESULTS AND DISCUSSION

### 4.1 Validation of Unsteady Pressure Distribution

Comparison of the first-harmonic pressure distribution along the girth at some transverse sections has been made in Kashiwagi *et al.*[1)], and its repeatability and reliability has been already confirmed. In particular, good agreement with CFD results on the nonlinear feature around the still waterline was remarkable.

As another validation of measured results, we have computed the first-harmonic wave-exciting forces from integration of unsteady pressure distribution measured in the diffraction problem and compared the result with the corresponding forces measured directly with dynamometer. The results are shown in Fig. 2, which shows also good agreement, indicating reliability of the unsteady pressure measured by means of FBG pressure sensors. We note however that there exist slight discrepancies in the surge exciting force at some wavelengths, which may be attributed to the scarcity of FBG sensors in the bow upper region above the still waterline. Despite not shown in this paper, the same kind of comparison was made for the radiation problem and very good agreement in the added mass and damping coefficient was also confirmed between the values by the pressure integration and the direct measurement with dynamometer.

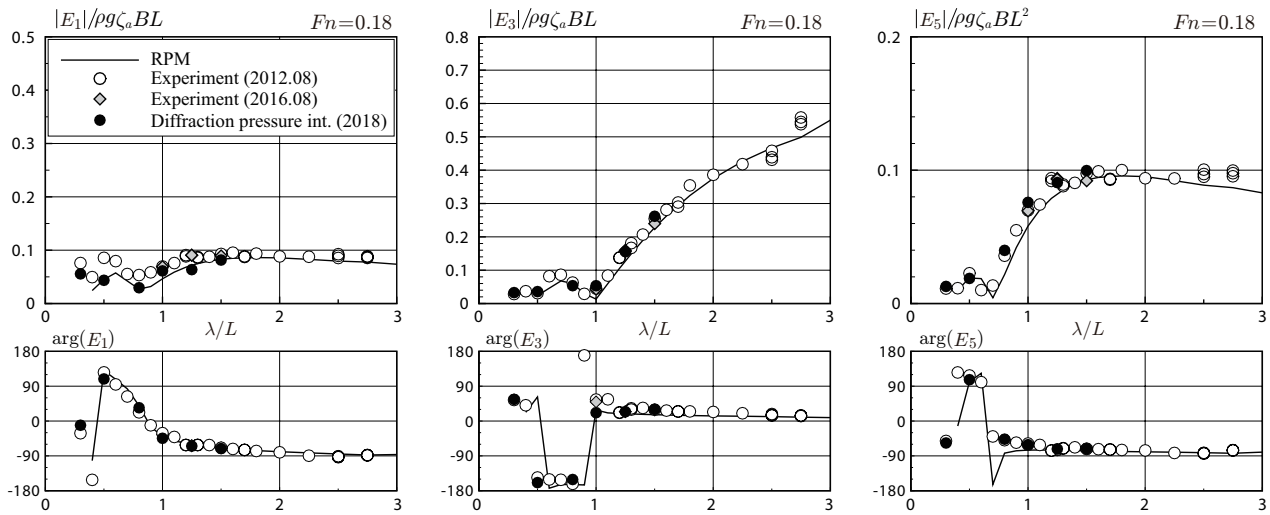


Fig. 2 Validation of pressure integration on the hull surface of RIOS bulk carrier in diffraction problem: comparison with the values measured directly by dynamometer at $Fn$ = 0.18 in head waves.

### 4.2 Vertical Bending Moment Distribution

We start with an easier case, i.e. at zero forward speed ($Fn$ = 0.0) in head waves. Since the wave steepness $H/\lambda$ in the experiment was set to about 1/50, measured phenomena must be in the framework of linear theory. Thus, a comparison for the longitudinal distribution of VBM is made between the value obtained from Eq. (1) using the measured data only and the value computed with RPM based on the linear potential theory. The results of comparison at $Fn$ = 0.0 are shown in Fig. 3 at wavelengths of $\lambda/L$ = 0.8, 1.0, 1.25, 1.5, and 2.0 for the maximum values in the hogging (plus) and sagging (minus) moments. Very good agreement can be confirmed for the sectional values of VBM between the experiment and RPM, implying that the unsteady pressure distribution on the ship-hull surface and the ship-motion RAO are also in good agreement.

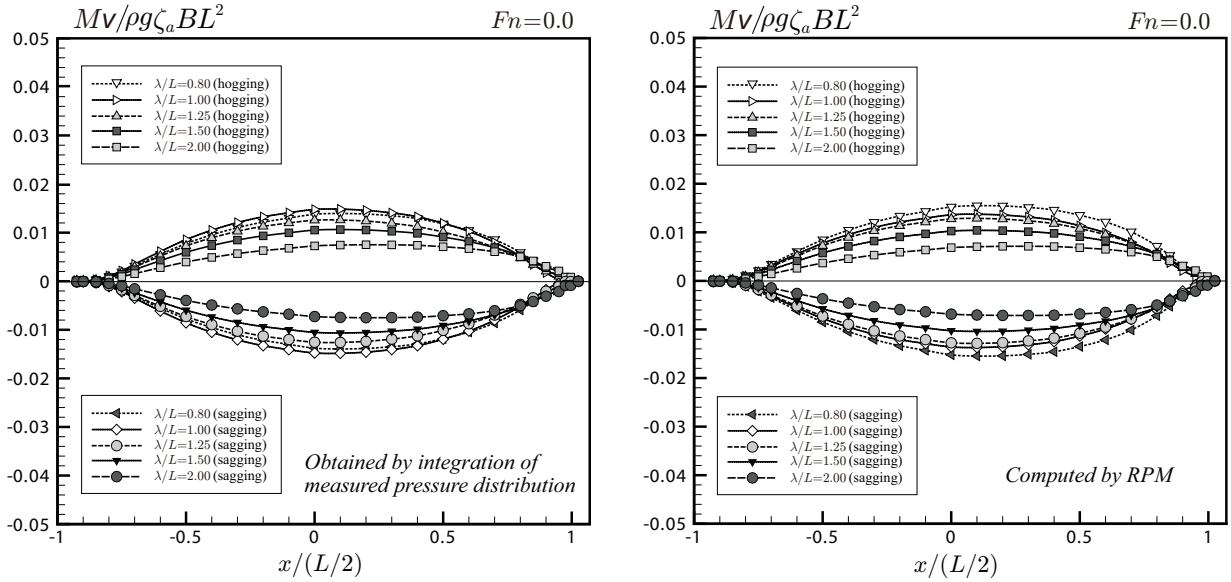


Fig. 3 Longitudinal distribution of vertical bending moment (VBM) on RIOS bulk carrier at $Fn$ = 0.0 in head waves. Left: integration of measured pressure distribution, Right: computed by RPM.

Next comparison is for the case of forward speed $Fn$ = 0.18, in which nonlinearity in the VBM must be observed especially when the ship motions are resonant around $\lambda/L$ = 1.25; that is, the magnitude in the sagging moment is larger than that in the hogging moment, although the wave steepness is the same as that at $Fn$ = 0.0. To see visually the degree of nonlinearity at $\lambda/L$ = 1.25, two snapshots for the wave profile at sagging and hogging conditions in the experiment are shown in Fig. 4. Since the degree of nonlinearity is relatively conspicuous, numerical computations at $Fn$ = 0.18 were implemented using CFD software, FINE/Marine. Shown in Fig. 5 is a comparison of the longitudinal distribution of VBM between the values evaluated only

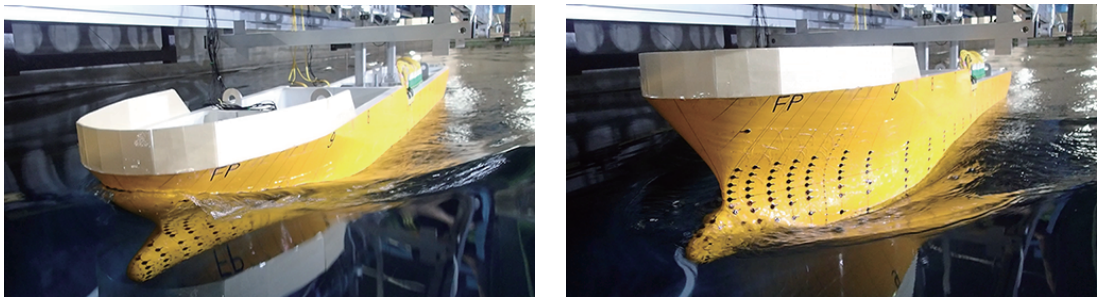


Fig. 4 Snap shots of wave profile at $\lambda/L = 1.25$ of head wave and $Fn = 0.18$. Left: sagging, Right: hogging.

with measured data and computed with CFD. (We note that, in the forward-speed case, the steady pressure due to forward movement of the ship is incorporated in the VBM computation.) From this comparison, we can see overall agreement between the experiment and CFD computation, although CFD results tend to overestimate slightly for some wavelengths, e.g. the hogging moment at $\lambda/L = 1.25$. More importantly, the asymmetric VBM can be clearly observed with larger sagging moment, and the position where the cross-sectional VBM becomes maximal is slightly shifted forward as compared to the case of $Fn = 0.0$; which can be attributed to the forward-speed effect that the magnitude of unsteady pressure becomes larger in the bow region at $Fn = 0.18$.

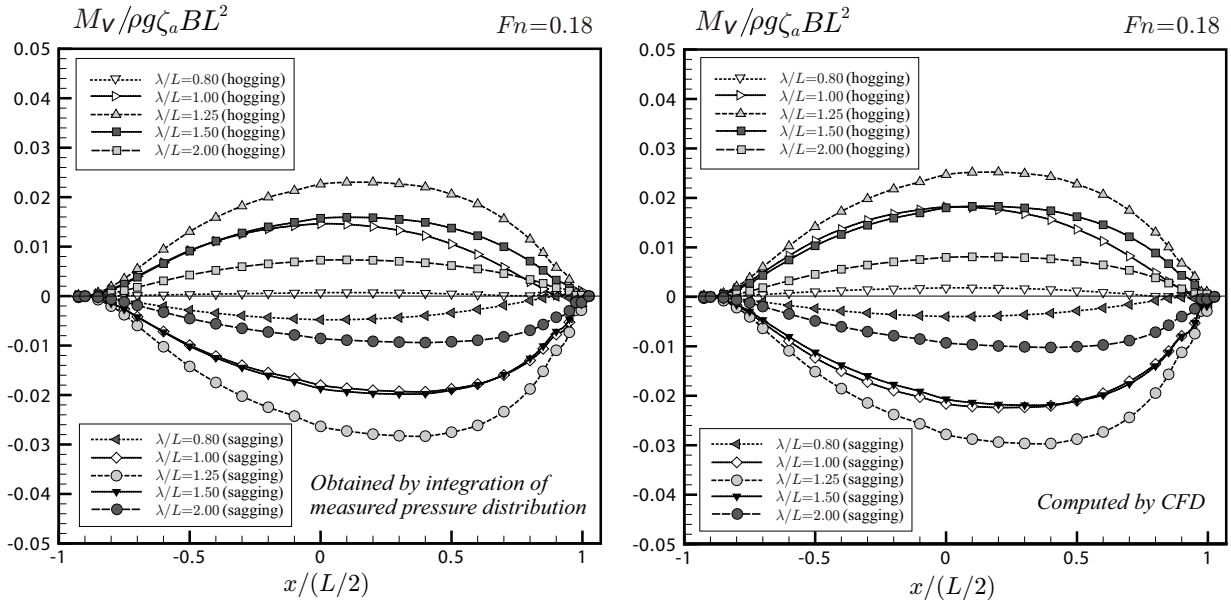


Fig. 5 Longitudinal distribution of vertical bending moment (VBM) on RIOS bulk carrier at $Fn = 0.18$ in head waves. Left: integration of measured pressure distribution, Right: computed by CFD.

## 5 CONCLUSION

By using the spatial distribution of unsteady pressure in head waves measured in 2018 with 333 FBG pressure sensors and also heave and pitch motions measured at the same time, the longitudinal distribution of VBM was obtained and compared with numerically computed results by RPM and CFD method. Good agreement could be confirmed at both $Fn = 0.0$ and 0.18, not only qualitatively but also quantitatively regarding nonlinear and forward-speed effects observed in the maximum values in the hogging and sagging moments. The results in this study may provide a new paradigm for obtaining the VBM experimentally at any transverse section and useful validation data for numerical computation methods.

## REFERENCES

1) Kashiwagi, M., Iwashita, H., Miura, S., Hinatsu, M.: Study on Added Resistance with Measured Unsteady Pressure Distribution on Ship-Hull Surface, Proceedings of 34th IWWWFB (Newcastle, Australia), pp. 81-84, 2019.

2) Iwashita, H., Kashiwagi, M., Ito, Y., Seki, Y., Yoshida, J., Wakahara, M.: Calculation of Ship Seakeeping in Low-Speed/Low-Frequency Range by Frequency-Domain Rankine Panel Methods (in Japanese), Journal of The Japan Society of Naval Architects and Ocean Engineers, No.24, pp. 129-146, 2017.